International Journal of
Intelligent Systems and
Applications in Engineering
ISSN:2147-6799 www.atscience.org/IJISAE
Advanced Technology and Science
Original Research Paper

A Mitigation Technique for Inrush Currents in Load Transformers for the Series Voltage Sag Compensator

B.Hari Prasad [1], P.Harsha Vardhan Reddy [1], Dr.M.Padma Lalitha *[1]

Received 24thJuly 2013, Accepted 17th November 2013

Abstract: In many countries, high-tech manufacturers concentrate in industry parks. Survey results suggest that 92% of interruption at industrial facilities is voltage sag related. An inrush mitigation technique is proposed and implemented in a synchronous reference frame sag compensator controller. The voltage sag compensator consists of a three phase voltage source inverter and a coupling transformer for serial connection. It is the most cost effective solution against voltage sags. When voltage sag happen, the transformers, which are often installed in front of critical loads for electrical isolation, are exposed to the disfigured voltages and a DC offset will occur in its flux linkage. When the compensator restores the load voltage, the flux linkage will be driven to the level of magnetic saturation and severe inrush current occurs. The compensator is likely to be interrupted because of its own over current protection. This paper proposes an inrush current mitigation technique together with a state-feedback controller for the Voltage sag compensator.

Keywords: *Voltage sag, flux linkage, inrush current, transformer, power quality, voltage sag compensator.*

1. Introduction

Power quality issues have received much attention in recent years. Therefore, any power quality events in the utility grid can affect a large number of manufactures. Records show that voltage sag, transients, and momentary interruption constitute 92% of the power quality problems [1].Voltage sags often interrupt critical loads and results in substantial productivity losses. Industries have adopted the voltage sag compensators as one of the most cost-effective ride-through solutions [2]–[7], and most compensators can accomplish voltage restoration within a quarter cycles. However, the load transformer is exposed under the deformed voltages before the restoration, and magnetic flux deviation may be developed within the load transformers. Once the load voltage is restored, the magnetic flux may further drift beyond the saturation knee of the core and lead to significant inrush current. The over current protection of the compensator could be easily triggered and lead to compensation failure. Various transformer inrush reduction techniques have been presented, like controlling power-on angle and the voltage magnitude [8], or actively controlling the transformer current [9]. These methods could easily alter the output voltage waveforms of the converter, and thus, is not suitable for voltage sag compensators, which demand precise point-on wave restoration of the load voltages.

2. Compensator Configuration.

The voltage sag compensator consists of a three-phase voltage-source inverter (VSI) and a coupling transformer for serial connection as shown in Fig.1.

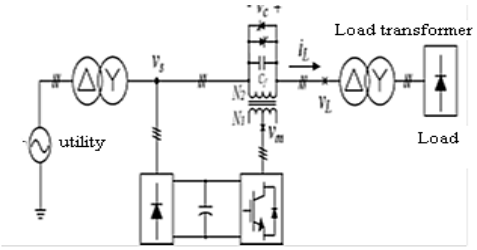

Figure 1. Simplified one Line diagram of the off line series voltage sag compensator

When the grid is normal, the compensator is bypassed by the thyristors for high operating efficiency. When voltage sags occur, the voltage sag compensator injects the required compensation voltage through the coupling transformer to protect critical loads from being interrupted. However, certain detection time (typically within 4.0 ms) is required by the sag compensator controller to identify the sag event [10]. And the load transformer is exposed to the deformed voltage from the sag occurrence to the moment when the compensator restores the load voltage. Albeit its short duration, the deformed voltage causes magnetic flux deviation inside the load transformer, and the magnetic saturation may easily occur when the compensator restores the load voltage, and thus, results in the inrush current. The inrush current could trigger the over current protection of the compensator and lead to compensation failure. Thus, this paper proposes an inrush mitigation technique by correcting the flux linkage offsets of the load transformer, and this technique can be seamlessly integrated with the state-feedback controller of the compensator.

2.1. Dynamics of the Sag Compensator.

The dynamics of the sag compensator can be represented by an equivalent circuit in Fig.2. Generally, the sag compensator is rated for

[1] *Department of Electrical & Electronics Engineering, Annamacharya Institute of Technology& science, India*
** Corresponding Author: Email: poreddyharshavardhan@gmail.com*

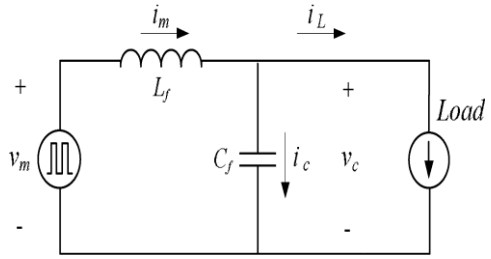

Figure 2. Per-phase equivalent circuit of the series voltage sag compensator

Compensating all three phase voltages down to 50% of nominal grid voltage. The coupling transformer is capable of electrical isolation or boosting the compensation voltage. Moreover, the leakage inductor of the coupling transformer is used as the filter inductor L_f and is combined with the filter capacitor C_f installed in the secondary winding of the coupling transformer to suppress pulse width modulated (PWM) ripples of the inverter output voltage v_m. The dynamics equations are expressed as follows

$$L_f \frac{d}{dt}\begin{bmatrix} i_{ma} \\ i_{mb} \\ i_{mc} \end{bmatrix} = \begin{bmatrix} v_{ma} \\ v_{mb} \\ v_{mc} \end{bmatrix} - \begin{bmatrix} v_{ca} \\ v_{cb} \\ v_{cc} \end{bmatrix} \quad (1)$$

$$c_f \frac{d}{dt}\begin{bmatrix} v_{ca} \\ v_{cb} \\ v_{cc} \end{bmatrix} = \begin{bmatrix} i_{ma} \\ i_{mb} \\ i_{mc} \end{bmatrix} - \begin{bmatrix} i_{La} \\ i_{Lb} \\ i_{Lc} \end{bmatrix} \quad (2)$$

Where $[V_{ma}V_{mb}V_{mc}]^T$ is the inverter output voltage, $[I_{ma}I_{mb}I_{mc}]^T$ is the filter inductor current, $[V_{ca}V_{cb}V_{cc}]^T$ is the compensation voltage, and $[I_{La}\ I_{Lb}\ I_{Lc}]^T$ is the load current. Equations (1) and (2) are transformed into the synchronous reference frame as the following:

$$\frac{d}{dt}\begin{bmatrix} i^e_{mq} \\ i^e_{md} \end{bmatrix} = \begin{bmatrix} 0 & -\omega \\ \omega & 0 \end{bmatrix}\begin{bmatrix} i^e_{mq} \\ i^e_{md} \end{bmatrix} + \frac{1}{L_f}\begin{bmatrix} v^e_{mq} \\ v^e_{md} \end{bmatrix} - \frac{1}{L_f}\begin{bmatrix} v^e_{cq} \\ v^e_{cd} \end{bmatrix} \quad (3)$$

$$\frac{d}{dt}\begin{bmatrix} v^e_{cq} \\ v^e_{cd} \end{bmatrix} = \begin{bmatrix} 0 & -\omega \\ \omega & 0 \end{bmatrix}\begin{bmatrix} V^e_{cq} \\ v^e_{cd} \end{bmatrix} + \frac{1}{c_f}\begin{bmatrix} i^e_{mq} \\ i^e_{md} \end{bmatrix} - \frac{1}{c_f}\begin{bmatrix} i^e_{Lq} \\ i^e_{Ld} \end{bmatrix} \quad (4)$$

where superscript "e" indicates the synchronous reference frame representation of this variable and ω is the angular frequency of the utility grid. Equations (3) and (4) show the cross-coupling terms between the compensation voltage and the filter inductor current. The block diagram of the physical circuit dynamics are illustrated in the right-hand side of Fig.3.

2.2. Voltage and Current Closed-Loop Controls

Fig.3 shows the block diagram of the proposed control method. Note that the d-axis controller is not shown for simplicity. The block diagram consists of the full state-feedback controller [12]and the proposed inrush current mitigation technique. The feedback control, feed forward control, and decoupling control are explained as follows.

1) Feedback Control: The feedback control is to improve the precision of the compensation voltage, the disturbance rejection capability, and the robustness against parameter variations. As shown in Fig.3.the capacitor voltage v^e_{cq} and the inductor current i^e_{mq} are handled by the outer-loop voltage control and the inner-loop current control, respectively. The voltage control is implemented by a proportional gain Kpv with a voltage command v^{e*}_{cq} produced by the voltage sag compensation scheme. The current control also consists of a proportional control gain Kpi to accomplish fast current tracking.

2) Feed forward Control: To improve the dynamic response of the

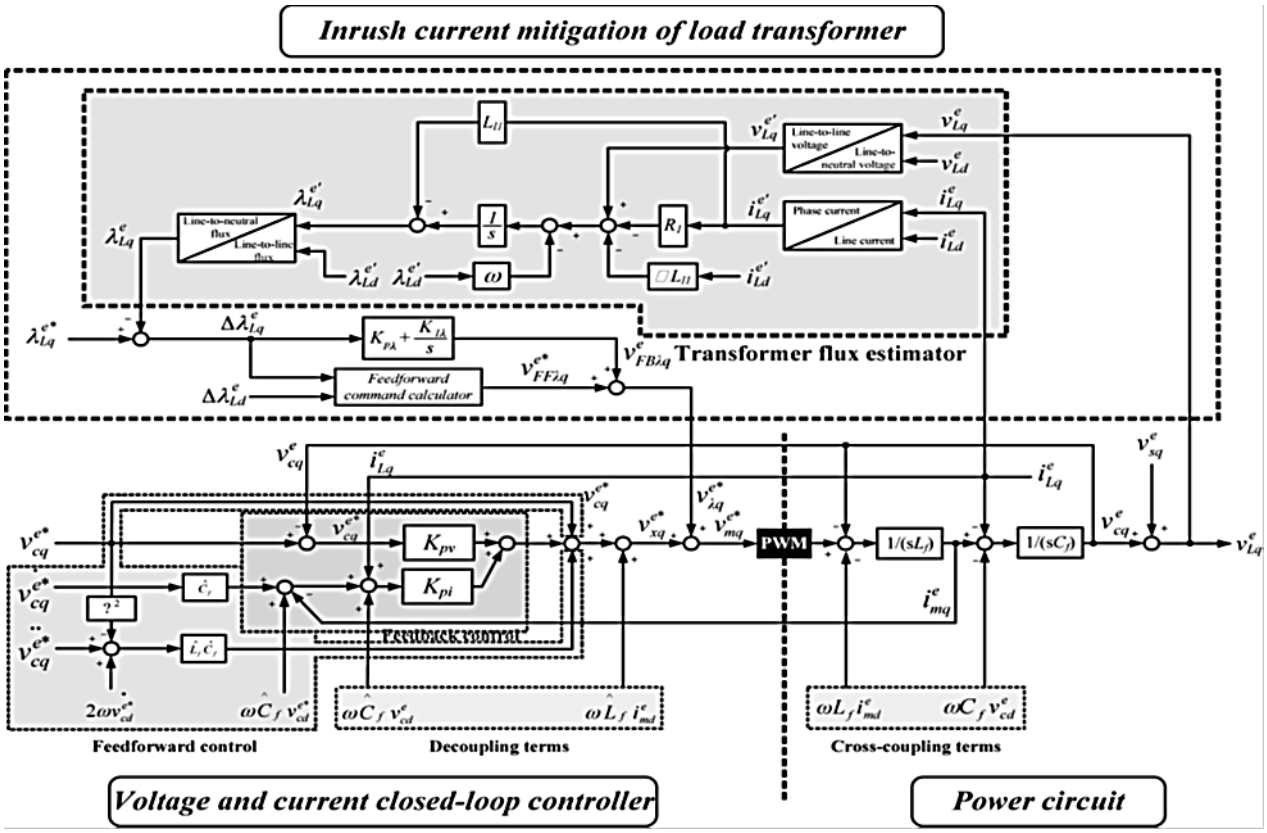

Figure 3. Block diagram of the proposed inrush current mitigation technique with the state-feedback control

voltage sag compensator, the feed forward control is added to the voltage controller to compensate the load voltage immediately when voltage sag occurs. The feed forward voltage command can be calculated by combining the compensation voltage and the voltage drop across the filter inductor L_f.

3) Decoupling Control: The cross-coupling terms are the result of the synchronous reference frame transformation, as in (3) and (4). The controller utilizes the decoupling terms to negate the cross coupling and reduce the interferences between the d–q axes. Fig. 3 shows that the decoupling terms can be accomplished by the filter capacitor voltage v^e_{cd}, the filter inductor current i^e_{md} and the estimated values of the filter capacitor and the filter inductor.

2.3. Inrush Current Mitigation Technique

1) Flux Linkage Deviation due to Sags: The flux linkage of the phase a and b winding is expressed as follows:

$$\lambda_{Lab}(t) = \int^{t} v_{Lab}(\tau)d\tau \tag{5}$$

Fig.5. illustrates the line-to-line voltage across the transformer winding and the resulting flux linkage from the sag occurrence to completion of the voltage compensation. When voltage sag occurs (t=tsag), The controller detects the sagged voltage and injects the required compensation voltage at t = taction. The flux linkage of the transformer winding a and b during the voltage compensation process can be expressed as following:

where v^*_{Lab} is the normal load voltage defined as follows

$$\lambda_{Lab}(t) = \lambda_{Lab}(t)_{t=tsag} + \int_{tsag}^{tactio_t} v_{Lab}(\tau)d\tau + \int V_{Lab}(\tau)d\tau \tag{6}$$

$$v^*_{Lab}(t) = v^*_{Lab}\sin\left(\omega t + \phi^*_{Lab}\right)\forall t$$

Equation (6) can be rewritten as follows:

$$\lambda_{Lab}(t) = \lambda_{Lab}(t)_{t=tsag} - \int_{0}^{tsag_t} v^*_{Lab}(\tau)d\tau + \int_{tsag}^{taction} (v_{Lab}(\tau) - v^*_{Lab}(\tau))d\tau + \int_{0}^{t} v^*_{Lab}(\tau)d\tau \tag{7}$$

where V^*_{Lab} is the magnitude of load voltage, ω is the grid frequency, and Φ^*_{Lab} is the phase angle. Thus, after the voltage compensation is completed, the flux linkage can be expressed as follows:

$$\lambda_{Lab}(t) = \Delta\lambda_{Lab}(t)_{t=taction} + \frac{v^*_{Lab}}{\omega}\sin\left(\omega t + \phi^*_{Lab} - \frac{\pi}{2}\right) \tag{8}$$

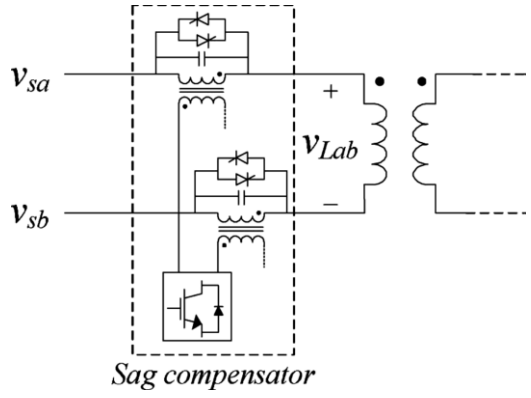

Figure 4. Connection diagram of the proposed system and the delta/wye load transformer

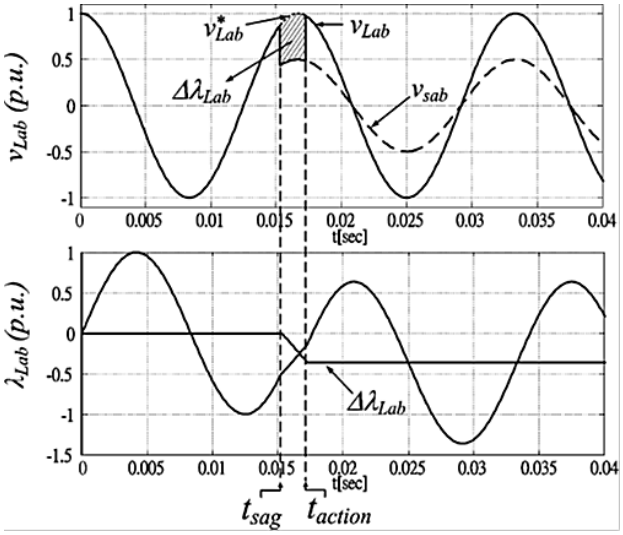

Figure 5. Transformer voltage and corresponding transient flux linkage

2) Design of the Flux Linkage Estimator: Fig.6 is a per phase model of a three-phase transformer under load, where R_1 and R_2 represent the copper losses, L_{11} and L_{12} are the equivalent leakage inductances, Rc represents the core losses, and Lm is the magnetizing inductance.

The dynamics equation of the load transformer can be represented in the synchronous reference frame as follows:

$$s\begin{bmatrix}\lambda^e_{mq}\\ \lambda^e_{md}\end{bmatrix} = \begin{bmatrix}v^e_{Lq}\\ v^e_{Ld}\end{bmatrix} - \left(R_1 + L_{l1}\right)s\begin{bmatrix}i^e_{Lq}\\ i^e_{Ld}\end{bmatrix}$$

$$- L_{l1}\begin{bmatrix}0 & \omega\\ -\omega & 0\end{bmatrix}\begin{bmatrix}i^e_{Lq}\\ i^e_{Ld}\end{bmatrix} - \begin{bmatrix}0 & \omega\\ -\omega & 0\end{bmatrix}\begin{bmatrix}\lambda^e_{Lq}\\ \lambda^e_{Ld}\end{bmatrix} \tag{9}$$

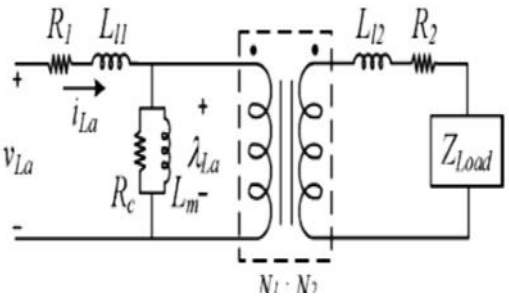

Figure 6. Equivalent per-phase circuit model of the load transformer

where the frequency ω (=377 rad/s) is the angular frequency of the utility grid A flux linkage estimator based on (9) can be implemented, as shown in Fig. 7. This transformer flux estimation scheme is applied to the proposed inrush mitigation technique, which includes the feedback and feed forward control of the flux linkage. The integration of voltage and current closed-loop controllers and the transformer flux estimator are shown in Fig.3.In the control block diagram, the flux estimator is used for the load transformer with delta–wye connection. Thus, a transformation from the line-to-neutral voltage to the line-to-line voltage is applied to obtain the voltages across the transformer windings. In practical applications, moreover, the integrator in the proposed flux estimator is usually implemented as the low-pass filter with an extremely low cutoff frequency (1/(s + ωc) to provide stability and avoid any accumulative errors caused by the signal offset from the transducers and the analog/digital converters. In the feedback control loop, the flux linkage command λ^{e*}_{Lq} is calculated based

on pre fault load voltage v^{e}_{Lq}, and the estimated flux linkage λ^{e}_{Lq} is generated by the flux linkage estimator in Fig.7.The error between λ^{e*}_{Lq} and λ^{e}_{Lq} is regulated by a PI regulator. To speed up the dynamics response of the inrush current mitigation, the estimated flux linkage deviation $\Delta\lambda^{e}_{Lq}$ ($=\lambda^{e*}_{Lq}-\lambda^{e}_{Lq}$) is also utilized as a feed forward control term. The feed forward command calculator can generate a suitable feed forward flux command according to the estimated flux linkage deviation $\Delta\lambda^{e}_{Lq}$ and $\Delta\lambda^{e}_{Ld}$ to accelerate the correction of flux linkage during the compensator starting transient. Details of the feed forward command calculator and the design process are given in [11].

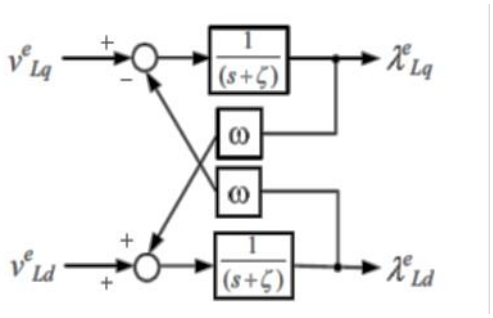

Figure 7. Proposed flux linkage estimator under the synchronous reference frame.

The flux linkage controller eventually produce the voltage command $V^{e*}_{\lambda q}$, as shown in Fig.3.The complete command voltages of the sag compensator is established by the summation of $V^{e*}_{\lambda q}$ and V^{e*}_{xq} (from the voltage and current closed-loop control

3. Simulation Results

A prototype voltage sag compensator with inrush
current mitigation technique is implemented in MATLAB. The one-line diagram is as given in Fig.1.

Fig. 8. shows that asymmetrical fault is introduced in utility line, and the simulation results of voltage sag compensator without the inrush current mitigation technique. The controller detects the voltage sag in 4.0ms after the fault occurs, and injects the required compensation voltage immediately to maintain load voltage in normal value as shown in Fig. 8(b). The transformer flux linkage DC offsets caused by the voltage sag can be clearly observed in Fig. 8(c), which results in a significant inrush current of peak value 14A as shown in Fig. 8(d). Fig. 8(e) shows the transformer flux linkage under the synchronous reference frame (λeLd). The voltage compensation process causes the flux linkage λeLd oscillate and naturally decays to the normal state by core losses of the transformer and the power consumption of the load.

Under the same asymmetrical fault, Fig. 9 shows

The simulation waveforms when the inrush current mitigation technique is utilized in compensation process. Fig. 9(a) and (b) illustrate proposed inrush current mitigation technique can achieve fast voltage compensation and without any flux linkage DC offset during the transient compared with Fig. 8(b) and (c). Therefore, the inrush current caused by the voltage sag can be avoided completely compared to Fig. 8(d). Furthermore, Fig. 9(a) also shows that the inrush current mitigation technique generates an extra voltage to correct the trace of transient flux linkage when the compensation is initiated compared to Fig. 8(c). The magnitude of the extra voltage is usually dependent on proportion gain KPλ. Fig.9(d) shows the tracking performance of proposed inrush current mitigation technique. The P-I regulator proposed method can be recognized as a virtual damper. A large number of KP can accelerate the flux linkage λLd to track the flux linkage command λ e*Ld. However, it may cause a high current in the start transient.

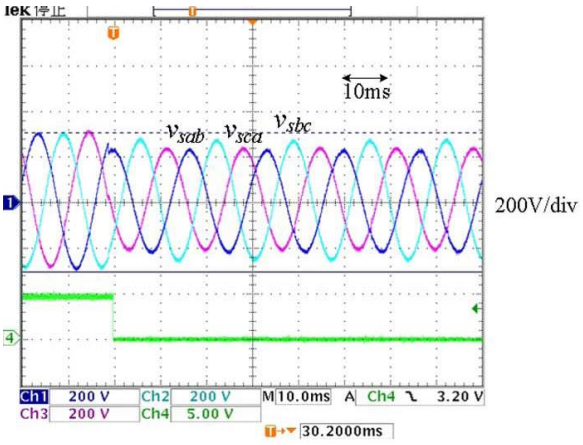

(a)

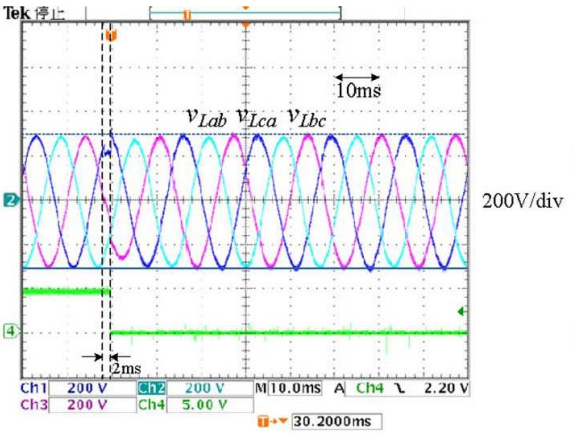

(b)

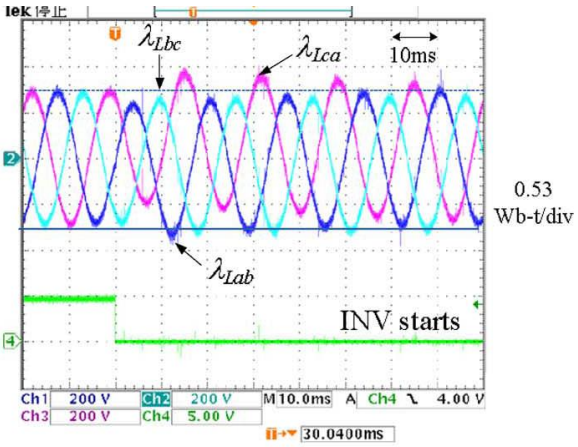

(c)

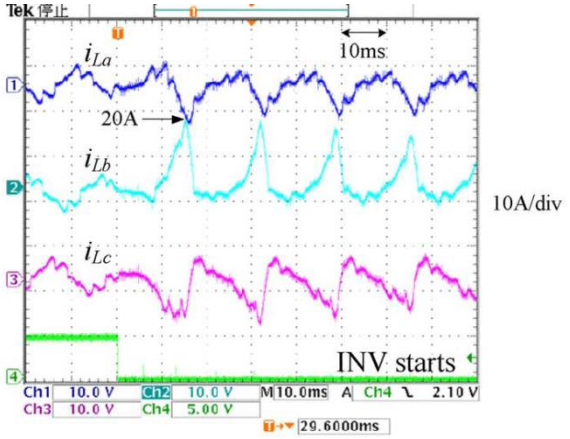

(d)

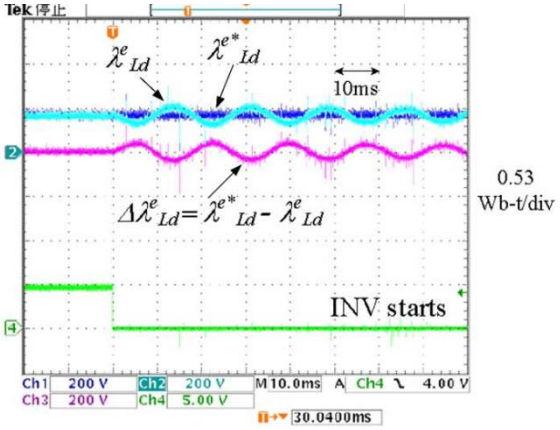

(e)

Figure 8. Test results under phase to phase voltage sag without the proposed inrush current mitigation technique. (a) Source voltage V_s. (b) Load voltage $V_{L\text{-}L}$ (c) Flux linkage of the load transformer $\lambda_{L\text{-}L}$ (d) Load current I_L (e) Flux linkage of d-axis λ^{e}_{Ld}

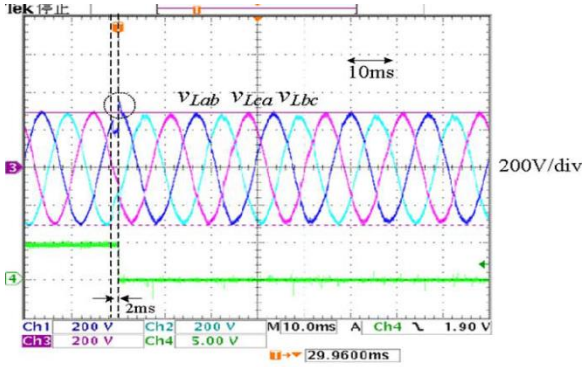

(a)

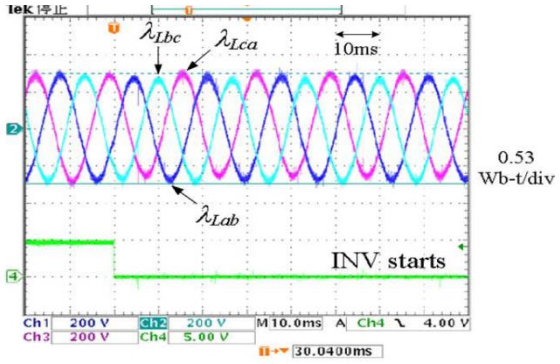

(b)

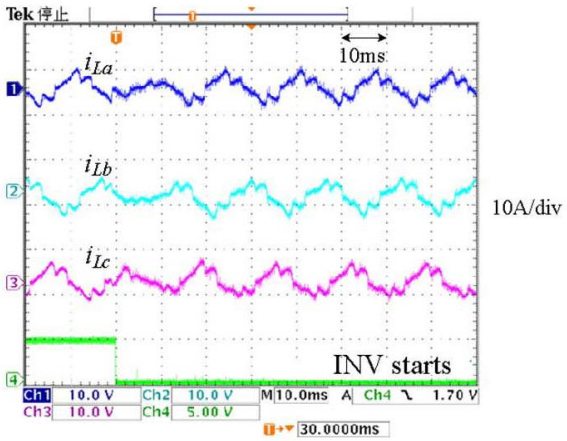

(c)

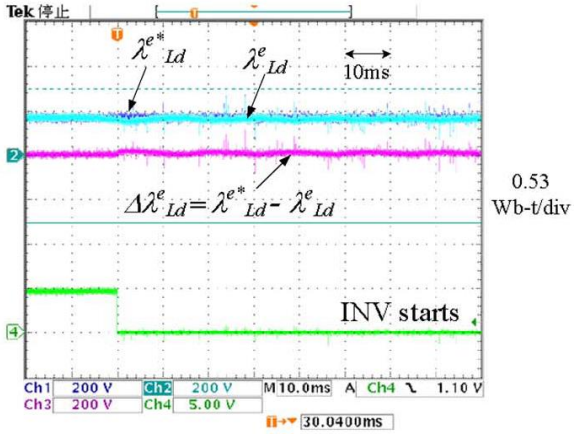

(d)

Figure 9. Test results under a phase to phase voltage sag with the inrush current mitigation technique. (a) Load voltage $V_{L\text{-}L}$. (b) Flux linkage of the load transformer $\lambda_{L\text{-}L}$. (c) Load current I_L (d) Flux linkage of d-axis λ^{e}_{Ld}

4. Conclusion

This paper proposes an inrush current mitigation technique incorporating with the full sate feedback controller to prevent the inrush current during the voltage compensation process. The controller includes a voltage control, a current control and a flux linkage control. The proposed control method is based on the synchronous reference frame which enables voltage sag compensator to achieve fast voltage injection and prevent the inrush current. When voltage sag occurs, the controller can track the transient flux linkage and calculate a required compensation voltage in real-time for fast compensation and elimination of flux linkage DC offset caused by voltage sags. It shows that the proposed control method provides a high disturbance rejection capability for voltage sag compensator compared with conventional voltage-current state feedback control method. The proposed method can be easily integrated with the existing voltage sag compensation control system without using any extra sensors.

References

[1] D. L. Brooks and D. D. Sabin, "An assessment of distribution system power quality," Elect. Power Res. Inst., Palo Alto, CA, EPRI Final Rep. TR-106249-V2, May 1996, vol. 2.

[2] W. E. Brumsickle, R. S. Schneider, G. A. Luckjiff, D. M. Divan, and M. F. McGranaghan, "Dynamic sag correctors: Cost-effective industrial power line conditioning," IEEE

Trans. Ind. Appl., vol. 37, no. 1, pp. 212–217, Jan./Feb. 2001.

[3] N. H. Woodley, "Field experience with dynamic voltage restorer (DVRTMMV) systems," in Proc.IEEE Power Eng. Soc. Winter Meeting, Jan. 23–27, 2000, vol. 4, pp. 2864–2871.

[4] R. Affolter and B. Connell, "Experience with a dynamic voltage restorer for a critical manufacturing facility," in Proc. IEEE Transmiss. Distrib. Conf. Expo., 2003, vol. 3, pp. 937–939.

[5] C. N.-M. Ho, H. S. H. Chung, and K. T. K. Au, "Design and implementation 20of a fast dynamic control scheme for capacitor-supported dynamic voltage restorers," IEEE Trans. Power Electron., vol. 23, no. 1, pp. 237–251, Jan. 2008.

[6] C. Meyer, R. W. De Doncker, Y. W. Li, and F. Blaabjerg, "Optimized control strategy for a medium voltage DVR—Theoretical investigations and experimental results," IEEE Trans. Power Electron., vol. 23, no. 6,pp. 2746–2754, Nov. 2008.

[7] J. G. Nielsen and F. Blaabjerg, "A detailed comparison of system topologies for dynamic voltage restorers," IEEE Trans. Ind. Appl., vol. 41, no. 5, pp. 1272–1280, Sep./Oct. 2005.

[8] M. S. J. Asghar, "Elimination of inrush current of transformers and distribution lines," in Proc. IEEE Power Electron., Drives Energy Syst. Ind. Growth, 1996, vol. 2, pp. 976–980.

[9] Y. Cui, S. G. Abdulsalam, S. Chen, and W. Xu, "A sequential phase energization technique for transformer inrush current reduction—Part I: Simulation and experimental results," IEEE Trans. Power Del., vol. 20, no. 2, pp. 943–949, Apr. 2005.

[10] W. Xu, S. G. Abdulsalam, Y. Cui, and X. Liu, "A sequential phase energization technique for transformer inrush current reduction—Part II: Theoretical analysis and design guide," IEEE Trans. Power Del., vol. 20, no. 2, pp. 950–957, Apr. 2005.

[11] P.C.Y. Ling and A. Basak, "Investigation of magnetizing inrush current in a single-phase transformer," IEEE Trans.Magn., vol. 24, no. 6, pp. 3217– 3222, Nov. 1988.

[12] C. Fitzer, A. Arulampalam, M. Barnes, and R. Zurowski, "Mitigation of saturation in dynamic voltage restorer connection transformers," IEEE Trans. Power Electron., vol. 17, no. 6, pp. 1058–1066, Nov. 2002.

International Journal of
Intelligent Systems and
Applications in Engineering
ISSN:2147-6799 www.atscience.org/IJISAE
Advanced Technology and Science
Original Research Paper

A simple Mathematical Fuzzy Model of Brain Emotional Learning to Predict *Kp* Geomagnetic Index

Ehsan Lotfi *[1], A. Keshavarz[2]

Received 2th October 2013, Accepted 3th December 2013

Abstract: In this paper, we propose fuzzy mathematical model of brain limbic system (LS) which is responsible for emotional stimuli. Here the proposed model is utilized to predict the chaotic activity of the earth's magnetosphere. Numerical results show that the correlation of the results obtained from the proposed fuzzy model is higher than non-fuzzy models. Hence, the proposed model can be applied in real time chaotic time series prediction.

Keywords: *Cognitive science, Amygdala, Computational model, Chaotic time series.*

1. Introduction

Emotions are cognitive processes and multidisciplinary studies of emotion have a long history. Form the psychological point of view, emotions can be derived with reward and punishment received from various real-life situations and studies of the neural basis of emotion culminated in the limbic system (LS) theory of emotion [1-4]. The LS processes the emotional stimuli [2-6] and is located in the cerebral cortex and consists of two main components including: amygdala and orbitofrontal cortex (OFC) (Figure 1). Amygdala is located in subcortical area and its main cognitive functions are long term memory and responsibility for emotional stimuli [7-8]. Amygdala receives connections from the sensory cortical areas [7-8] and also interacts with the OFC that tries to prevent inappropriate responses from the amygdala [7-8]. Recently, researchers have tried to present mathematical models of LS. The first applied mathematical model of LS was proposed by Morén and Balkenius [7-8] which is a neuropsychological motivated mathematical model. This basic model and its modified versions [9-10] have been utilized in various applications including: control application, prediction and alarm systems [11-19]. A control algorithm based on LS model was introduced by Lucas et al. [9-10] which is an action generation mechanism based on sensory inputs and emotional cues. Also LS model was proposed as an alarm system to predict the *Kp* index of geomagnetic activity [19-22] and to predict the *AE* index of space weather phenomena [23]. These indices characterize the solar winds and geomagnetic storms that is a complex system and can greatly disturb communication systems and damage satellites [23]. The *Kp* have chaotic behaviour and can be considered as time series. Recently we proposed a mathematical model of LS for classification and pattern recognition problems [24-25] and in this paper we fuzzify the model and propose fuzzy computational model of LS to predict *Kp* index. A fuzzy framework can better explain the brain behaviour. Hence we fuzzify the connections in the LS model and implement the inhibitory task of OFC as a fuzzy decision making layer. The proposed model is presented in Section 2 and Section 3 presents a comparison between proposed method, Basic LS model and ANN (Artificial Neural Network) [26] which is popular predictor in geomagnetic phenomena forecasting.

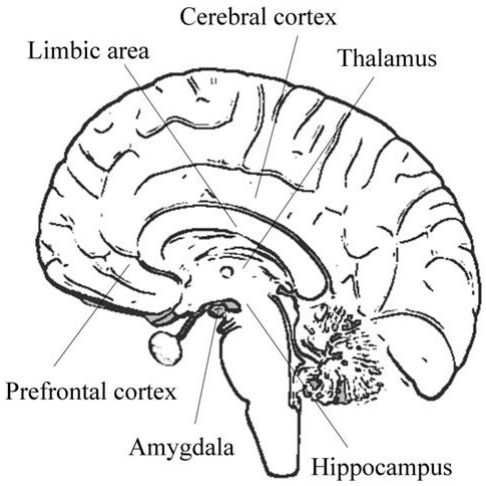

Figure 1. The LS in the brain (from [25])

2. Proposed fuzzy computational model of LS

The main modifications introduced here with respect to previous models are considering the plastic connections as some fuzzy rules and defining a fuzzy decision making layer on the final output of LS model as illustrated in Figure 2. In the figure solid lines present the data flow and learning lines are presented as dashed lines. According to the amygdala-orbitofrontal interaction, the proposed computational model named FDBEL (Fuzzy Decay Brain Emotional Learning) is divided into the two parts. The amygdaloidal part receives fuzzy inputs from the thalamus and from cortical areas, while the orbital part receives fuzzy inputs from the sensory cortex only. Also OFC has a fuzzy output that prevents the wrong answers of amygdala. The system also receives a fuzzy reinforcing signal. We improve the performance

[1] *Department of Computer Engineering, Torbat-e-Jam Branch, Islamic Azad University, Torbat-e-Jam, Iran*
[2] *Department of Psychology, Torbat-e-Jam Branch, Islamic Azad University, Torbat-e-Jam, Iran*
** Corresponding Author: Email: esilotf@gmail.com*

of the model by using decay rate γ in amygdale learning rule. So the learning rules are as follow:

$$v_i^{k+1} = (1-\gamma).v_i^k + \alpha.\max(T_i^{k+1} - E_a^k, 0).s_i^k \quad (1)$$

$$w_i^{k+1} = w_i^k + \beta.(s_i^k . R_0) \quad (2)$$

where k is learning step and R_0 is internal reward calculated by:

$$R_0 = \begin{cases} \max(E_a'^k - R^k, 0) - E_a^k, if\ R^k \neq 0 \\ \max(E_a'^k - E_o^k), otherwise \end{cases} \quad (3)$$

In this model each plastic connection between thalamus and amygdala and between sensory cortex and thalamus, are considered as a fuzzy rule. The Takagi Sugeno fuzzy model for i[th] amygdala connection is as follow:

If (S_i is V_i) then (A_i=S_i.v_i)

The (S_i) is i[th] input and (V_i) is i[th] fuzzy set with bell-shaped membership function where the (v_i) locates the center of the curve. So the output of amygdala (E_a) is calculated by following formula:

$$E_a = \sum_i A_i(s_i; v_i, a, b) \quad (4)$$

And E'_a in learning rule (see Eq. 8) is:

$$E'_a = \sum_{i, i \neq th} A_i(s_i; v_i, a, b) \quad (5)$$

where

$$A_i(s_i; v_i, a, b) = \frac{1}{1 + |\frac{s_i - v_i}{a}|^{2b}} \cdot s_i \cdot v_i \quad (6)$$

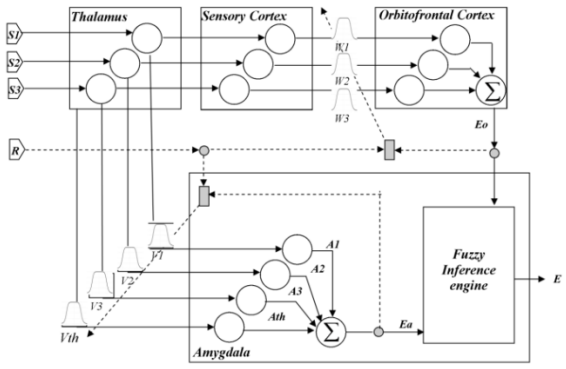

Figure 2. Proposed fuzzy computational model of LS

Also the Takagi Suginio fuzzy model for i[th] OFC connection is as follow:

If (S_i is W_i) then (O_i=S_i.w_i)

Where (S_i) is i[th] sensory input and (W_i) is i[th] fuzzy set with (w_i) center bell-shaped membership function. So the output of OFC (E_o) is calculated by following formula:

$$E_a = \sum_i O_i(s_i; w_i, a, b) \quad (7)$$

where

$$O_i(s_i; w_i, a, b) = \frac{1}{1 + |\frac{s_i - w_i}{a}|^{2b}} \cdot s_i \cdot w_i \quad (8)$$

The outputs of amygdala and OFC are crisp values. We fuzzify the output of OFC as a Gaussian membership function with mean E_o which is input of fuzzy inference engine. So the final output (E) fire using following rule:

$$E = 1 - e^{\frac{-(E_a - E_o)^2}{2c^2}} \quad (9)$$

Where the subtraction between amygdala output (E_a) and OFC output (E_o) implements the inhibitory task of OFC.

3. Experimental Results

To test the offered method, the chaotic time series of *Kp* characterized the geomagnetic activity of the earth's magnetosphere, was collected from National Space Science Data Center (NSSDC). Totally 184104 hourly samples from 1976 to 1996 has been downloaded. We extract each 4 sequence samples as a pattern and 5th as its target. So 184099 pattern-target pairs of *Kp* index extracted. The official values of *Kp* index are as following form:

0 '0+'1–'1 '1+'2–'2 '2+'···'9

To adjust the weights we scaled all of data between 0 and 1. For all learning scenarios listed below α and β (Eqs. 6,7) are set at 0.2 and 0.8 respectively. To find optimized decay rate, consider the following scenario: by decay rate 0 system trained the samples in 1988. This training is repeated 10 times and the average of errors recorded. This scenario is repeated by various values (For γ = 0, 0.05, 0.1, 0.15, 0.2, …,1.0). The highest error is obtained using γ = 0 and the lowest error obtained by using γ = 0.05. The parameters values used in learning phase presented in Table 1. In Eq. (6); the values a and b are set at (v_i-0.5) and (v_i-0.25), respectively. In Eq. (8); a = (w_i-0.5), b = (w_i-0.25) and finally in Eq. 9; c = (E_o-0.25).

Table 1. the value parameters used in learning phase

Parameter	Value
α	0.8
β	0.2
γ	0.01

To assess the FDBEL method, 15% of samples are used as validation, 15% as test and 70% as training samples. Figure 3 present the regression plots of the results obtained from FDBEL. In the figures, R is regression value of data. According to the figure the correlations of results in test set, validation and training set are more than 0.85.

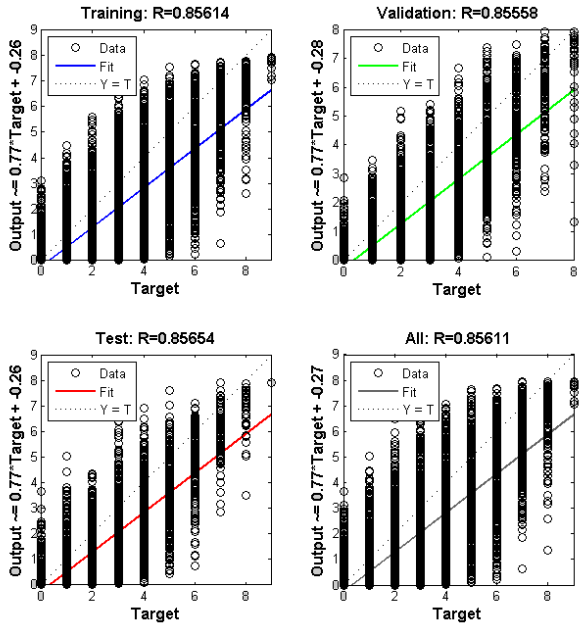

Figure 3. The regression plots of the *Kp* prediction results in the training set, test set and validation set separately obtained from FDBEL

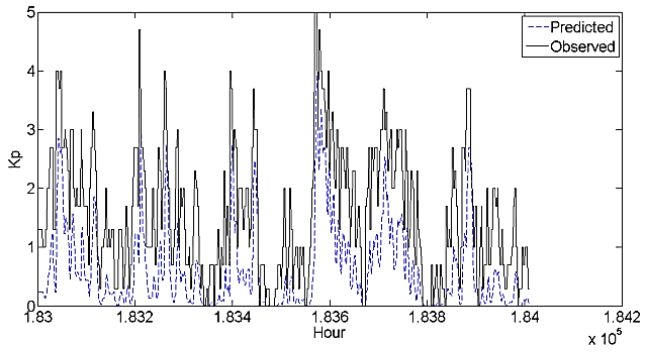

Figure 4. Observed and predicted values at last 1000 hours year 1996 obtained from FDBEL

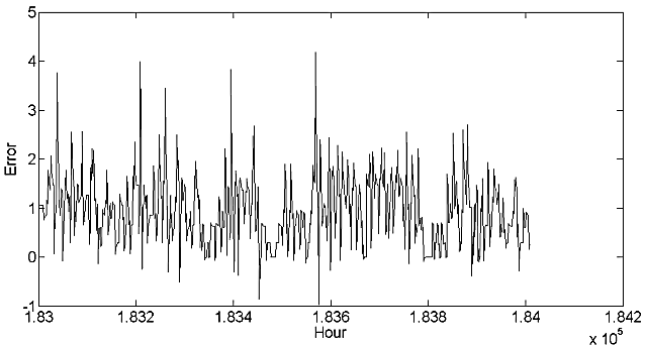

Figure 5. Prediction error at last 1000 hours year 1996 obtained from FDBEL

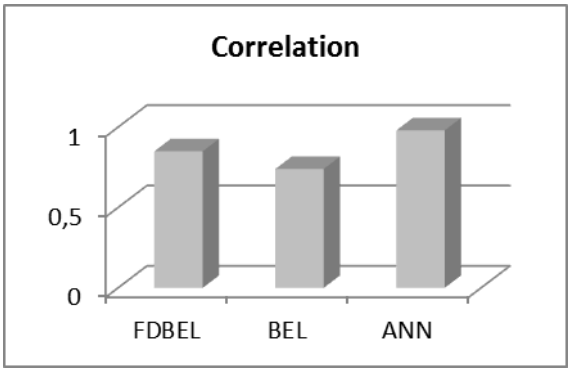

Figure 6. The correlation coefficient comparison between three methods

Figure 4 shows the observed and predicted values of the last 1000 hours *Kp* time series obtained from FDBEL. The error size is illustrated in the Figure 5. Finally Figure 6 presents a comparison between FDBEL, BEL and ANN, based on correlation coefficient. The stop criterion in learning process of all methods was validation check and the value COR = 0.85 obtained from FDBEL and significantly increased with respect to the BEL. ANN based predictor shows high correlation in the prediction results. But the number of learning epochs of ANN was 100 while it was just 3 for FDBEL.

4. Conclusions

In this paper we presented fuzzy model of limbic system named FDBEL and utilized to predict *Kp* geomagnetic index. This index characterizes solar storms or sub storms that is a complex system with chaotic behavior. The main modifications introduced with respect to the previous models are considering the amygdala and OFC plastic connections as some fuzzy rules and defining inhibitory task of OFC as fuzzy decision maker layer on the final output. The experimental results show that proposed model can forecast the *Kp* time series with high correlation and low computational complexity. According to the number of epochs in learning phase, the main feature of FDBEL is fast training. Also the comparison between FDBEL, BEL and the ANN based predictor presents that high correlation in least number of learning epochs is obtained from FDBEL.

References

[1] J. Morén, Emotion and Learning - A Computational Model of the Amygdala, Lund University Cognitive Studies, 2002.

[2] J. E. LeDoux, "Emotion circuits in the brain," Annual Review of Neuroscience, Vol. 23, pp. 155-184, 2000.

[3] J. E. LeDoux, The Emotional Brain, Simon and Schuster, New York, 1996.

[4] E. T. Rolls, "Neurophysiology and functions of the primate amygdala," In: The Amygdala: Neurobiologycal Aspects of Emotion, Memory and Mental Dysfunction, New York, Wiley-Liss, pp. 143-165. 1992.

[5] L. Cahill, R.J. haier, J. Fallon, "Amygdala activity at encoding correlated with long-term, free recall of emotional information," Proceedings-National Academy of Science USA, Vol. 93, pp. 8015-8021, 1996.

[6] A Bechara, H Damasio, AR Damasio "Different contributions of the human amygdala and Ventromedial Prefrontal Cortex to Decision-Making," Journal of Neuroscience, Vol. 19, pp. 5473–5481, 1999.

[7] C. Balkenius, J. Morén, "Emotional learning: a computational model of amygdala," Cybernetics and

Systems, Vol. 32, pp. 611-636, 2001.

[8] J. Morén, C. Balkenius, "A computational model of emotional learning in the amygdala," In: From Animals to Animats 6: Proceedings of the 6th International Conference on the Simulation of Adaptive Behaviour, Meyer, J.A., A. Berthoz, D. Floreano, H.L. Roitblat and S.W. Wilson (Eds.). MIT Press, Cambridge, MA., USA., pp. 115-124, 2000.

[9] C. Lucas, D. Shahmirzadi and N. Sheikholeslami, "Introducing BELBIC: brain emotional learning based intelligent controller," International Journal of Intelligence Automotive Soft Computing, Vol. 10, pp. 11-21, 2004.

[10] C. Lucas, "BELBIC and its industrial applications: towards embedded neuroemotional control codesign," Integrated Systems, Design and Technology, Vol. 3, pp. 203-214, 2010.

[11] H. Rouhani, M. Jalili, B.N. Araabi, W. Eppler, C. Lucas, "Brain emotional learning based intelligent controller applied to neurofuzzy model of micro-heat exchanger," Expert System and Application, Vol. 32, pp. 911-918, 2007.

[12] M. Samadi, A. Afzali-Kusha, C. Lucas, "Power management by brain emotional learning algorithm," 7th International Conference on ASIC, pp. 78 – 81, 2007.

[13] E. Daryabeigi, G.R.A. Markadeh, C. Lucas, "Emotional controller (BELBIC) for electric drives — A review," 36th Annual Conference on IEEE Industrial Electronics Society, pp. 2901 – 2907, 2010.

[14] M. Chandra, Analytical Study of A Control Algorithm Based on Emotional Processing, M.S. Dissertation, Indian Institute of Technology Kanpur, 2005.

[15] C. Lucas, R.M. Milasi, B.N. Araabi, "Intelligent modeling and control of washing machine using Locally Linear Neuro-Fuzzy (LLNF)," Asian Journal of Control, Vol. 8, pp. 393-400, 2006.

[16] S. Jafarzadeh, R. Mirheidari, M.R.J. Motlagh, M. Barkhordari, "Designing PID and BELBIC controllers in path tracking troblem," International Journal of Computers Communications & Control, Vol. 3, pp. 343-348, 2008.

[17] A. Sadeghieh, H. Sazgar, K. Goodarzi, C. Lucas, "Identification and real-time position control of a servo-hydraulic rotary actuator by means of a neurobiologically motivated algorithm," ISA Transactions, Vol. 51, pp. 208-219, 2012.

[18] A. M. Khalilian, Abedi, A.D. Zadeh,"Position control of hybrid stepper motor using brain emotional controller," Energy Procedia, Vol. 14, pp. 1998-2004, 2012.

[19] A. Gholipour, Lucas, C. A. R. O., & Shahmirzadi, D. A. N. I. A. L. (2004), "Predicting geomagnetic activity index by brain emotional learning," WSEAS AIKED, 3.

[20] E. Lotfi and Akbarzadeh-T, M. R., (2012). "Supervised brain emotional learning," IEEE Int. Joint Conf. on Neural Networks (IJCNN), pp. 1-6, doi: 10.1109/IJCNN.2012.6252391

[21] E. Lotfi and Akbarzadeh-T., M. R., (2014), "Adaptive Brain Emotional Decayed Learning for Online Prediction of Geomagnetic Activity Indices," Neurocomputing, doi: 10.1016/j.neucom.2013.02.040

[22] E. Lotfi, M. R. Akbarzadeh-T., 2013. "Emotional Brain-Inspired Adaptive Fuzzy Decayed Learning for Online Prediction Problems," In Proc. IEEE International conference on fuzzy systems (FUZZ-IEEE 2013), July 7-10 2013, Hyderabad, India.

[23] T. Babaie, Karimizandi, C. Lucas, "Learning based brain emotional intelligence as a new aspect for development of an alarm system," Soft Comput., Vol. 12, pp: 857–873, 2008.

[24] E. Lotfi, M. R. Akbarzadeh-T., 2013. "Brain Emotional Learning Based Pattern Recognizer," Cybernetics & Systems, doi: 10.1080/01969722.2013.789652

[25] E. Lotfi, 2013. "Mathematical modeling of emotional brain for classification problems," Proceedings of Institute of Applied Mathematics, Vol. 2, No. 1, 2013.

[26] M. T. Hagan, H.B. Demuth, M.H. Beale, Neural Network Design, Boston, MA: PWS Publishing, 1996.